# Previously unaccounted atmospheric mercury deposition in a midlatitude deciduous forest

Daniel Obrist[a,1], Eric M. Roy[a], Jamie L. Harrison[b], Charlotte F. Kwong[c], J. William Munger[d], Hans Moosmüller[e], Christ D. Romero[a], Shiwei Sun[a,f], Jun Zhou[a], and Róisín Commane[b,c]

[a]Department of Environmental, Earth, and Atmospheric Sciences, University of Massachusetts Lowell, Lowell, MA 01854; [b]Lamont–Doherty Earth Observatory, Columbia University, Palisades, NY 10964; [c]Department of Earth and Environmental Sciences, Columbia University, New York, NY 10027; [d]Harvard John A. Paulson School of Engineering and Applied Sciences, Harvard University, Cambridge, MA 02138; [e]Division of Atmospheric Sciences, Desert Research Institute, Reno, NV 89512; and [f]State Key Laboratory of Cryospheric Science, Northwest Institute of Eco-Environment and Resources, University of Chinese Academy of Sciences, Lanzhou 730000, China

Edited by William H. Schlesinger, Cary Institute of Ecosystem Studies, Millbrook, NY, and approved May 13, 2021 (received for review March 21, 2021)

**Mercury is toxic to wildlife and humans, and forests are thought to be a globally important sink for gaseous elemental mercury (GEM) deposition from the atmosphere. Yet there are currently no annual GEM deposition measurements over rural forests. Here we present measurements of ecosystem–atmosphere GEM exchange using tower-based micrometeorological methods in a midlatitude hardwood forest. We measured an annual GEM deposition of 25.1 μg · m$^{-2}$ (95% CI: 23.2 to 26.7 1 μg · m$^{-2}$), which is five times larger than wet deposition of mercury from the atmosphere. Our observed annual GEM deposition accounts for 76% of total atmospheric mercury deposition and also is three times greater than litterfall mercury deposition, which has previously been used as a proxy measure for GEM deposition in forests. Plant GEM uptake is the dominant driver for ecosystem GEM deposition based on seasonal and diel dynamics that show the forest GEM sink to be largest during active vegetation growing periods and middays, analogous to photosynthetic carbon dioxide assimilation. Soils and litter on the forest floor are additional GEM sinks throughout the year. Our study suggests that mercury loading to this forest was underestimated by a factor of about two and that global forests may constitute a much larger global GEM sink than currently proposed. The larger than anticipated forest GEM sink may explain the high mercury loads observed in soils across rural forests, which impair water quality and aquatic biota via watershed Hg export.**

dry deposition | mass balance | mercury cycling

Mercury is a neurotoxic environmental pollutant distributed via the atmosphere to ecosystems globally (1). In terrestrial ecosystems, dry deposition of atmospheric gaseous elemental mercury (GEM) is considered the dominant source of mercury, accounting for 54 to 94% of mercury loads observed in soils (2–5). Terrestrial GEM deposition propagates through watersheds and ultimately provides a critical source of mercury to freshwater, coastal sediments, and marine biota (6). Yet, direct measurement of GEM dry deposition is lacking over most ecosystem types, in particular over forests, which are considered the largest global atmospheric GEM sink (7, 8). GEM deposition includes direct uptake of atmospheric GEM by plants, which is transferred to soils as litterfall when plants die off and shed leaves or as throughfall when precipitation washes it off from plant surfaces (9). Depending on environmental conditions, underlying soils serve as either additional sinks or as sources (i.e., emissions) of GEM to or from the atmosphere, which complicates quantification of integrated, whole-ecosystem net GEM loadings (10). Globally, dry GEM deposition to terrestrial ecosystems may constitute the largest removal mechanism of atmospheric mercury, currently estimated between 1,500 to 2,145 Mg · yr$^{-1}$ (6) and on average may turn over the entire global atmospheric mercury pool of 4,400 to 5,300 Mg (11) every 2 to 3.5 y.

Major uncertainties exist in regard to magnitude and seasonality of the dominant terrestrial GEM deposition and their controlling ecological and environmental controls. Data are particularly scarce from forests in which direct GEM exchange measurements are limited largely to summertime (12) or stem from Hg-contaminated sites (13, 14). Direct flux measurements are also required to partition GEM deposition into canopy and forest floor (litter and soil) contributions. In lieu of direct GEM flux measurements, GEM deposition across forests is often inferred from proxy measures such as mercury litterfall collected under canopies (8, 15). Litterfall mercury deposition, however, is not an ideal proxy for GEM dry deposition because it does not capture uptake by large woody tissues, nonvascular plants (i.e., lichen, mosses), and underlying soils, and it does not account for GEM re-emission back to the atmosphere after deposition (7). Here, we employed a micrometeorological flux-gradient method that directly quantifies GEM exchange at the ecosystem level over a 470-d record (May 2019 to August 2020) in a rural temperate forest in Massachusetts. The site is a second-growth forest that is actively accumulating biomass and is approaching standing biomass levels of old-growth stands in the region (16). The flux-gradient method we employed consists of GEM concentration measurements at two heights above the canopy in combination with quantification of atmospheric

## Significance

**Direct measurements of atmospheric deposition of gaseous elemental mercury (GEM) over a temperate forest showed a pronounced annual deposition of 25.1 μg · m$^{-2}$, which dominated as a source of mercury. GEM deposition was five times greater than wet deposition and three times greater than litterfall deposition, which has been used as a proxy for GEM deposition until now. Measured GEM deposition is driven by combined plant GEM uptake and underlying forest floor GEM uptake. Global forests may be a much larger global GEM sink than currently assumed, which may explain high mercury levels in soils across forests. Forest mercury mobilizes via watershed runoff and bioaccumulates in aquatic biota, ultimately leading to mercury exposures in wildlife and humans.**

Author contributions: D.O. and R.C. designed research; D.O., E.M.R., J.L.H., C.F.K., J.W.M., C.D.R., S.S., J.Z., and R.C. performed research; H.M. contributed new reagents/analytic tools; D.O., E.M.R., J.L.H., C.F.K., J.W.M., C.D.R., J.Z., and R.C. analyzed data; and D.O., E.M.R., J.L.H., C.F.K., H.M., J.Z., and R.C. wrote the paper.

The authors declare no competing interest.

This article is a PNAS Direct Submission.



[1]To whom correspondence may be addressed. Email: daniel_obrist@uml.edu.

This article contains supporting information online at https://www.pnas.org/lookup/suppl/doi:10.1073/pnas.2105477118/-/DCSupplemental.

Published July 16, 2021.

turbulence to calculate forest-level surface–atmosphere exchanges (17). We here analyze seasonality and diel patterns of GEM exchange, compare its magnitude to other deposition measurements such as litterfall and wet deposition, and assess contributions by the underlying forest floor using a second flux-gradient system deployed under the canopy.

## Results and Discussion

**Whole-Ecosystem GEM Exchange and Correlation to Vegetation Activity and $CO_2$ Assimilation.** Monthly averaged GEM fluxes showed atmospheric GEM deposition (negative exchange fluxes) during 12 of the 16 mo of measurements, with rates of deposition largest in summer and fall (August to November). We observed emissions to the atmosphere (positive fluxes) only during two winter and two spring months (May and December 2019 and January and April 2020), while small rates of deposition were observed during the rest of winter and springtime (Fig. 1 *A*–*C*). GEM fluxes showed strong diel variability, particularly in summer with large GEM deposition during midday up to 28 ng · $m^{-2}$ · $hr^{-1}$, compared to nighttime deposition maxima of 6 ng · $m^{-2}$ · $hr^{-1}$ (Fig. 2 and *SI Appendix*, Table S1). Different diel patterns emerged in spring when deposition dominated during nighttime, which reversed to emissions during daytime (e.g., in March and April 2020). In winter, there was smaller diel variability of GEM fluxes which remained relatively constant throughout the day. Wintertime snow cover quickly disappeared during the first 10 days of March 2020, but we did not observe a change in GEM flux dynamics before and after snow disappearance (Fig. 1*C*). Cumulative GEM exchange started with emissions in May 2019, which reversed quickly to deposition during the 2019 growing season and resulted in a substantial cumulative GEM deposition by end of November 2019. Winter months showed partial GEM emissions of about one-quarter of the previous summertime GEM deposition. In June 2020, GEM deposition resumed and strengthened throughout the second summer until the end of measurements in mid-August 2020. Cumulative net GEM deposition (i.e., all deposition minus emissions) between May 1, 2019, to August 12, 2020 (470 d), totaled 34.9 μg · $m^{-2}$ (Fig. 2*C* and Table 1), with a 95% CI of 33.0 to 37.2 9 μg · $m^{-2}$ (*SI Appendix*). Annual GEM deposition was 25.1 μg · $m^{-2}$ with a 95% CI of 23.2 to 26.7 μg · $m^{-2}$.

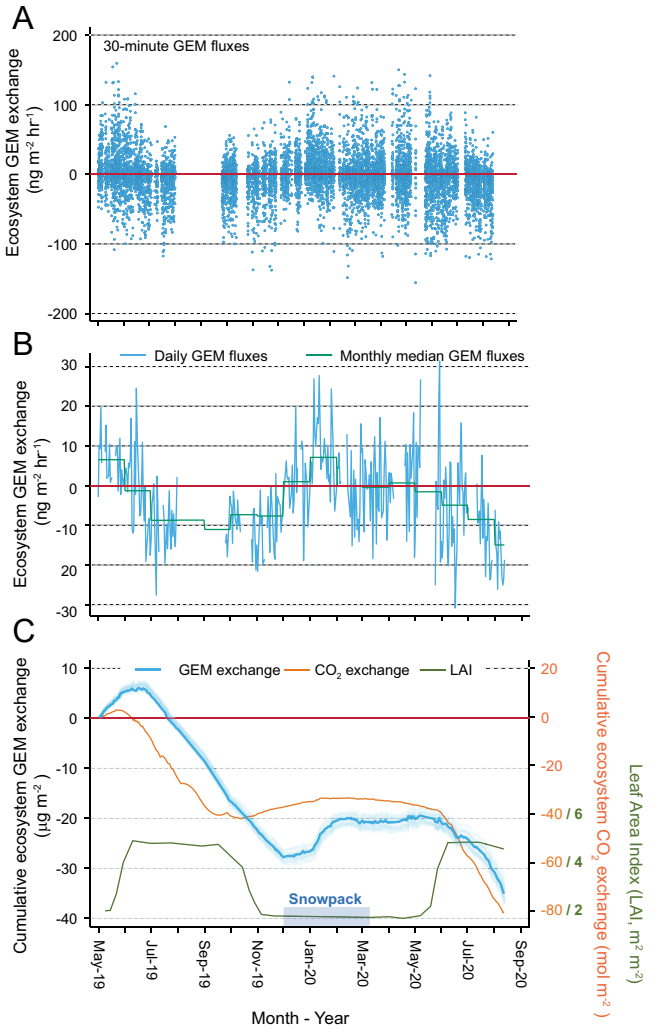


**Fig. 1.** (*A*) 30-min resolution GEM exchange fluxes measured over Harvard Forest. Negative fluxes denote deposition, and positive fluxes represent emissions. (*B*) Daily mean GEM fluxes and median monthly GEM fluxes (green lines). (*C*) Cumulative sums of daily fluxes of GEM and $CO_2$ starting on May 1, 2019. Missing flux values were interpolated using median monthly values. Shaded lines represent 95% CIs based on random error analysis as described in *SI Appendix*. Corresponding patterns of LAI are shown together with the $CO_2$ fluxes on the secondary *y*-axis.

We attribute these seasonal and diel GEM exchange patterns to vegetation uptake of GEM. Both seasonal and diel GEM flux patterns are similar to those of $CO_2$ fluxes, which generally exhibit large growing season and midday deposition due to photosynthetic $CO_2$ assimilation by plants (18). As a result, seasonal and diurnal fluxes show a coupling between the exchanges of GEM and $CO_2$. Seasonally, both GEM and $CO_2$ fluxes showed pronounced growing-season deposition while winter and early spring showed either emissions or near-zero fluxes (Fig. 1*C*). The only notable discrepancy between seasonal GEM and $CO_2$ flux patterns was observed in November 2019 ($CO_2$ showing emissions while GEM fluxes showing strong deposition). It is notable that snow cover started on December 1, 2019, after which the active forest GEM sink ceased, suggesting that the forest floor also served as a GEM sink. Not including November, median monthly GEM fluxes linearly correlated with forest $CO_2$ fluxes ($r^2$ = 0.52). During the active vegetation season between June and October, $CO_2$ fluxes also explained 49% of the diel flux variability of GEM based on linear regressions between median monthly fluxes for each hour of the day. In support of an active role of vegetation for GEM deposition, GEM fluxes were correlated with forest leaf area index (LAI; $r^2$ of 0.61 not including November), and GEM fluxes were statistically different at LAI above 3 $m^2$ · $m^{-2}$ (average depostion of 2.3 ng · $m^{-2}$ · $h^{-1}$) compared to LAI below 3 $m^2$ · $m^{-2}$ (average emission of 2.6 ng · $m^{-2}$ · $h^{-1}$). In addition, monthly GEM fluxes linearly correlated with air temperatures ($r^2$ of 0.49) and soil temperatures (e.g., at 5-cm depth, $r^2$ of 0.57) showing increased deposition during the warmer growing seasons.

Atmospheric GEM assimilation by vegetation has been reported by many studies (review by ref. 6), for example, based on experimental and stable isotope studies (2–5, 19, 20) and seasonal and interhemispheric atmospheric GEM fluctuations (21–23). We here show that strong growing-season net GEM deposition, aided by vegetation uptake, drives cumulative annual GEM deposition and dominates over other co-occurring GEM exchanges. Specifically, GEM fluxes are known to show bidirectional exchanges with co-occurring emissions and deposition over soils and plant surfaces and fractional re-emissions of GEM after deposition (24). Net GEM emissions were limited to a few months in winter and spring only, indicating that the forest largely retained deposited GEM, which is in contrast to strong GEM emissions that have been reported over agricultural fields and barren soils (10). GEM emissions in spring occurred before vegetation was fully active (e.g., May 2019 and March and April 2020) and peaked at midday, which is consistent with photochemical reduction and thermal desorption processes (10, 25).

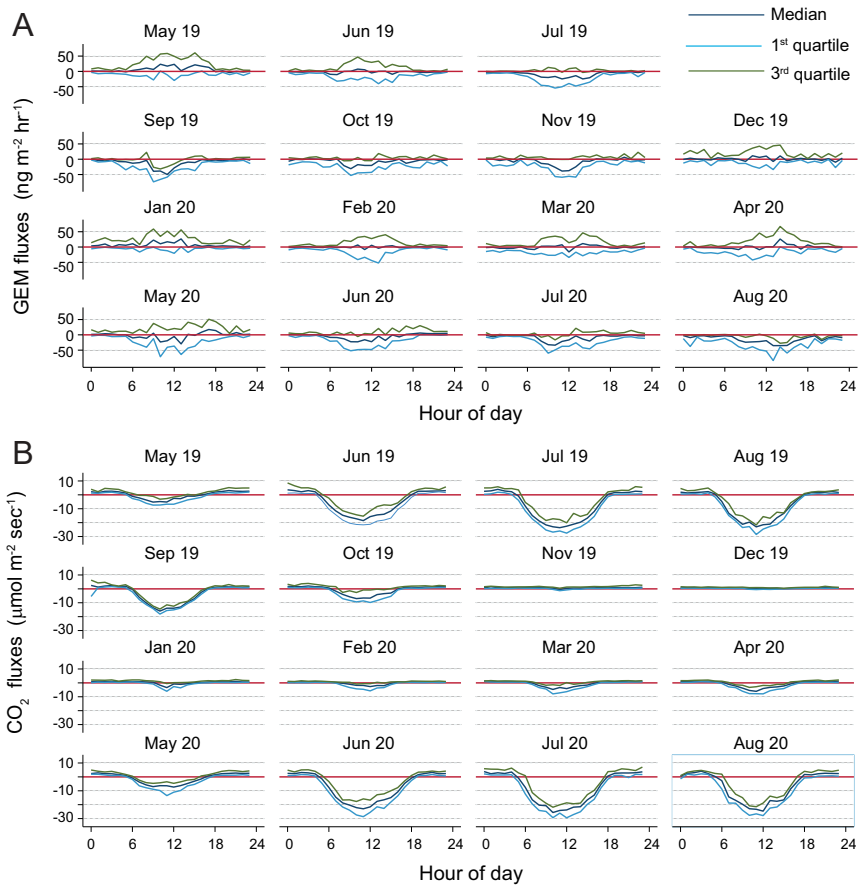


**Fig. 2.** (*A*) Diel patterns of ecosystem-level GEM exchange fluxes shown as monthly hourly median fluxes and upper and lower quartile ranges. (*B*) Corresponding diel patterns of monthly hourly median fluxes of $CO_2$.

GEM emission, however, largely ceased as the canopy began to leaf out and as emerging daytime GEM assimilation by plants dominated during active growing seasons and led to midday summertime deposition maxima.

**Forest-Floor GEM Exchange.** We quantified forest-floor GEM fluxes to assess their contributions to ecosystem-level GEM exchange using a second flux-gradient deployed above the forest floor (Fig. 3). Forest-floor GEM fluxes indicated consistent GEM deposition throughout the year (Fig. 3), suggesting that soil and litter served as additional ecosystem sinks of GEM. Forest-floor GEM uptake may include direct uptake and subsequent oxidation of GEM in soils (26) and GEM uptake in overlying litter layers (27). The observed deposition of atmospheric GEM to the forest floor could explain reported increases in Hg levels in litter during decomposition (27–29). Comparing cumulative flux patterns of the forest floor to that of ecosystem-level fluxes implies that limited periods of net GEM emissions at

**Table 1. Summary of annual and seasonal GEM deposition and associated 95% CIs based on error propagation shown in *SI Appendix***

| Species/process | Time period | Source | Deposition ($\mu g \cdot m^{-2}$) |
|---|---|---|---|
| GEM dry deposition | Study duration (470 d): May 1, 2019 to August 12, 2020 | This study | 34.9 (33.0 to 37.2) |
| GEM dry deposition | Annual (365 d) | This study | 25.1 (23.2 to 26.7) |
| GEM dry deposition | Growing season: Jun 1 to Sep 30, 2019 | This study | 21.9 (20.9 to 23.1) |
| Litterfall deposition | Annual | This study | 8.1 |
| GOM dry deposition | Annual | This study: GOM ∅ conc. of 4.1 ± 5.6 pg · $m^{-3}$ × $v_d$ | 1.9 |
| PHg dry deposition | Annual | Average of North America (35) | 1.1 |
| Wet Hg deposition | Annual | From NADP 2020, regional average | 5.0 |
| Total Hg deposition | Annual | Dry (GEM + GOM + PHg) + wet deposition | 33.1 |
| % GEM of total Hg deposition | Annual | | 76% |

Additional estimates and constraints of wet and dry deposition of other major atmospheric mercury species are based on additional measurements and published literature data.

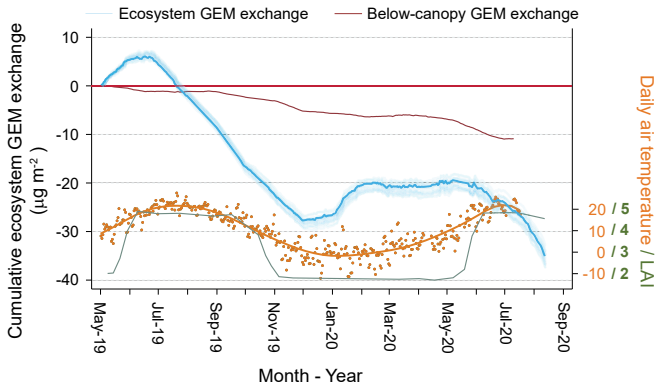


**Fig. 3.** Cumulative sum of ecosystem-level and forest-floor GEM exchanges. Forest-floor GEM fluxes are quantitatively uncertain due to application of the flux-gradient method below canopies and should be viewed as a measure of underlying flux direction. Shaded lines represent 95% CIs based on random error analysis as described in *SI Appendix*. Corresponding patterns of LAI (in meters$^2$ leaf area and meters$^{-2}$ ground surface area) and daily air temperatures (in °Celsius; line represents smoothed data) are shown on the secondary *y*-axis.

the ecosystem level in winter and spring are not caused by emissions from the underlying forest floor but may stem from above-ground tissues. Mixed forests maintain significant above-ground surface areas even during nonactive growing seasons due to woody biomass surfaces and coniferous needles, as evident by LAI which never dropped below 1.7 $m^2 \cdot m^{-2}$ at this site (Fig. 1*C*). Forest-floor GEM deposition could also explain GEM deposition at the ecosystem level during nighttime and possibly the discrepancy between $CO_2$ and GEM fluxes in November 2019 when photosynthetic $CO_2$ uptake largely ceased while GEM continued to show GEM deposition. Accumulating forest litter in fall may further shield soil surface from incident solar radiation and reduce the potential for soil GEM emission. Full quantitative flux partitioning between canopy and forest floor contributions, however, was not feasible in this study because of different footprints of measurements (i.e., range of meters above the forest floor compared to a few hundred meters above the forest). In addition, magnitudes of forest-floor flux-gradient measurements may be unreliable when turbulence near the ground is weak and intermittent, and thus, the underlying assumptions for valid flux-gradient calculations are not met (30). We hence primarily use below-canopy GEM fluxes to indicate GEM flux direction from the underlying forest floor (i.e., emission or deposition) rather than full quantitative constraints.

**GEM Deposition Studies over Other Terrestrial Ecosystems.** The only previous ecosystem-level GEM flux study over a rural forest we know of was conducted over several months (June through October) in a deciduous maple forest in Connecticut. Using a relaxed eddy accumulation approach (12), the study provided evidence of GEM deposition in forests with an estimated growing season GEM deposition of 5.6 $\mu g \cdot m^{-2}$, compared to a much larger deposition of 25.1 $\mu g \cdot m^{-2}$ (range of 23.2 to 26.7 $\mu g \cdot m^{-2}$) from June 1 through October 31 in our study. The study suggests to possibly have underestimated growing season GEM uptake as they missed early leaf-out GEM deposition fluxes. In contrast to our study, the study reported GEM emissions in late summer and fall (August through October), and flux magnitudes were much higher and more variable than our measurements. Reasons for differences in GEM flux patterns include a different methodological approach, possible footprint contributions by surrounding open grassland in the Connecticut study, and proximity to more urban areas. Other studies reported forest GEM fluxes over mercury-contaminated forests in the United States (13) and China (14) and showed predominantly GEM emissions to the atmosphere. The contrasting patterns of these studies are not surprising given that fluxes over mercury-contaminated areas strongly shift toward emissions (10, 25) and hence are not representative of GEM exchanges over rural ecosystems.

Only a few studies reported annual GEM fluxes over other ecosystem types. A total 2 y of GEM fluxes data over a tundra in northern Alaska (4) showed annual GEM deposition of 6.8 and 6.1 $\mu g \cdot m^{-2} \cdot yr^{-1}$, respectively, compared to the annual deposition of 25.1 $\mu g \cdot m^{-2}$ (range of 23.2 to 26.7 $\mu g \cdot m^{-2}$) in our forest. Annual GEM deposition over a temperate grassland in Switzerland was 25.4 $\mu g \cdot m^{-2} \cdot yr^{-1}$ when using the flux-gradient method (31). Another grassland site dominated by grasses, brush, and dispersed trees after a recent forest clearing in Maryland reported a small annual GEM deposition of 3.3 $\mu g \cdot m^{-2} \cdot yr^{-1}$ (32). Finally, an annual GEM flux study using relaxed eddy accumulation technique over a peatland in northern Sweden, a site with little vegetation growth, showed an annual net emission of GEM of 9.4 $\mu g \cdot m^{-2} \cdot yr^{-1}$ (33). Most available GEM flux studies over terrestrial sites hence show an annual net GEM deposition, which in our deciduous forest was comparable to a productive grassland, higher than annual GEM deposition in an arctic tundra and a recently converted grassland, and in opposite direction to a reported GEM emission of a peatland.

**Annual Deposition and Mass Balance Considerations.** Cumulative GEM deposition shows that the mixed hardwood forest in Massachusetts served as a substantial GEM sink of 34.9 $\mu g \cdot m^{-2}$ (range of 33.0 to 37.2 $\mu g \cdot m^{-2}$) over the duration of 470 d of measurements with an annual GEM deposition of 25.1 $\mu g \cdot m^{-2} \cdot yr^{-1}$ (range of 23.2 to 26.7 $\mu g \cdot m^{-2}$). GEM deposition was by far the dominant source of mercury deposition (Table 1). It is important to note, however, that measuring small GEM fluxes against the relatively larger atmospheric background was challenging at the level of a forest ecosystem and resulted in substantial flux variability and uncertainty ranges (*SI Appendix*, Table S1 and Fig. S5). Detailed analyses of high-resolution data by means of frequency and autocorrelation analyses (*SI Appendix*, Figs. S2 and S3), consistent and repeatable seasonal and diel patterns (Figs. 1 and 2), and error propagation based on random error analysis of time-repeated measurements (*SI Appendix*, Fig. S5) provided high confidence in the reliability of our GEM flux measurements. Cumulative GEM exchange also showed similar seasonal flux patterns between the two years of measurements.

Mercury wet deposition by rain and snow is monitored across the United States by the National Atmospheric Deposition Program (34) and is about 5 $\mu g \cdot m^{-2} \cdot yr^{-1}$ in this region based on interpolated deposition maps for the year 2017. We constrained dry deposition of gaseous oxidized mercury (GOM) based on limited measurements of GOM concentrations in late spring and early summer (*SI Appendix*, Fig. S6) which averaged 4.1 ± 5.6 $pg \cdot m^{-3}$ and yields a GOM deposition flux of 1.9 ± 2.6 $\mu g \cdot m^{-2} \cdot yr^{-1}$ if extrapolated to a full year. This estimated GOM deposition at Harvard Forest is smaller than an average GOM deposition of 6.4 $\mu g \cdot m^{-2} \cdot yr^{-1}$ estimated across North America (35), which is reasonable given that the North American average includes urban sites with higher GOM concentrations from anthropogenic emissions while our forest ecosystem is a rural site. We did not measure particulate mercury (PHg) deposition but assume an upper limit of 1.1 $\mu g \cdot m^{-2} \cdot yr^{-1}$ of deposition, which is the average PHg deposition reported across North America (35). These comparisons strongly suggest that GEM dry deposition was by far the dominant deposition pathway in this forest accounting for 76% of a total annual mercury deposition of about 33.1 $\mu g \cdot m^{-2} \cdot yr^{-1}$ (Table 1). The contributions of GEM to total

deposition are surprisingly similar to an estimate of 71% GEM contributions in an Alaskan tundra (4) and agree with stable mercury isotope analyses that indicate atmospheric GEM-derived sources to account for 57 to 94% of mercury in forest soils across North America (2, 5).

Litterfall mercury deposition has been used as a proxy measure to estimate dry deposition fluxes in forests (36). Litterfall data across 23 forest sites in the United States have shown average litterfall mercury deposition of 12.3 $\mu g \cdot m^{-2} \cdot yr^{-1}$ (range of 3.8 to 18.8 $\mu g \cdot m^{-2} \cdot yr^{-1}$) notably exceeding corresponding wet deposition that averaged 9.6 $\mu g \cdot m^{-2} \cdot yr^{-1}$ across the same region (37). We estimated litterfall mercury deposition at Harvard Forest using end-of-season foliage mercury concentration of four dominant tree species multiplied by a 10-y record of litterfall biomass fluxes (Table 2). Our results show litterfall mercury deposition of 8.1 $\mu g \cdot m^{-2} \cdot yr^{-1}$ that is about 3.1 times lower than measured annual GEM dry deposition. Using net daily $CO_2$ uptake to delineate periods of active vegetation growing periods (i.e., June 1 to October 1), the cumulative growing season dry deposition GEM sink amounted to 21.9 $\mu g \cdot m^{-2}$ (range of 20.9 to 23.1 $\mu g \cdot m^{-2}$) (Tables 1 and 2), which is 2.7-fold the value of litterfall mercury deposition, providing evidence that forest-level GEM uptake strongly exceeds litterfall deposition. This finding supports previous reports that large additional deposition fluxes in addition to foliar litterfall and wet deposition are needed to explain observed mercury accumulation in soils along a glacier retreat chronosequence (38).

**Implications for Global and Regional Mercury Cycling.** Our measurements of annual GEM deposition suggest that GEM deposition in forests is strongly underestimated. Total global terrestrial GEM deposition currently is estimated at 1,500 to 1,800 $Mg \cdot yr^{-1}$ (6). Global annual litterfall deposition, currently estimated in the range of 1,020 to 1,230 $Mg \cdot yr^{-1}$ (8, 39) would amount to a global GEM deposition of 3,162 to 3,813 $Mg \cdot yr^{-1}$ if GEM deposition exceeds litterfall deposition by a similar factor of 3.1 across other forests. The major reasons for higher deposition likely include unaccounted for GEM assimilation by vegetation and direct GEM uptake by the forest floor and soil. The forest GEM deposition sink at Harvard Forest may be enhanced by ongoing biomass growth and carbon sequestration driven by forest regrowth, climate warming, and increasing wetting and atmospheric $CO_2$ concentrations (16). Additional pathways of atmospheric GEM deposition include wash-off of GEM from plant surfaces and deposition via throughfall and stemflow deposition (38). A potentially larger and unaccounted for forest GEM sink will require major revision of other global pool sizes, atmospheric deposition and emission fluxes, and respective residence times in these environmental compartments. A larger than anticipated forest GEM sink also is consistent with strong mercury enhancements in soils across forests, which on average are 2.5 times higher than in barren soils (40, 41). High-soil mercury pools subsequently lead to water quality impairments via terrestrial runoff (42) and impact air quality when remobilized via wildfire emissions (43). Whole-ecosystem GEM fluxes across global forests and other ecosystems are needed to corroborate the strong GEM uptake observed in this midlatitude deciduous forest and constrain GEM sinks across global biomes.

## Materials and Methods

**Study Site and Ecosystem Characteristics.** The measurement site is located in a temperate deciduous hardwood forest at Harvard Forest research station near Petersham, Massachusetts (42°32′N, 72°11′W), at an elevation of 340 m with an annual average precipitation of 1,071 mm and a mean annual temperature of 6.6 °C. Cold winter temperatures result in wintertime snow cover with a peak snow water equivalent of 82 mm in 2020 (February 19) and an average peak snow water equivalent of 98 mm since 2009. The site houses a 31-m-tall flux tower near a climate-controlled hut for instrumentation with power and network access. Average tree height is about 24 m with vegetation dominated by red oak (*Quercus rubra*) representing about 80% of the tree basal area and other major species including red maple (*Acer rubrum*) and hemlock (*Tsuga canadensis*). Forest ages at this site range from 85 to 125 y with few trees exceeding 200 y of age (16). Nearly all forests in the region are second-growth after large-scale forest clearing in the mid-1800, and a major hurricane damaged about 70% of the standing timber in 1938. Soils are Spodosols (suborder Orthods) formed over sandy loam glacial till. Near-continuous forest extends several kilometers in all directions with no occupied dwelling closer than 2 km distance, beyond which the area is also forests and sparsely populated. The nearest highway is about 5 km distant.

**Micrometeorological Measurements.** The site has been used for micrometeorological measurements since 1990 and is home to the longest available $CO_2$ flux Eddy Covariance (EC) dataset in the world (44). The site facilitates excellent micrometeorological flux measurements with local energy budget closures within 20% (45). The flux-gradient approach (30) consists of GEM gradient measurements at two heights above the canopy multiplied by a measure of atmospheric turbulence and provides an aerially integrated flux over a whole ecosystem. GEM fluxes ($F_{GEM}$) are equal to gradients of a trace gas scaled by the rate of turbulent exchange according to the formula:

$$F_{GEM} = -K \times \Delta C_{GEM}/_{\Delta z} \quad (46),$$

where K equals the vertical turbulent exchange coefficient (also termed eddy diffusivity; units of $meters^2 \cdot second^{-1}$) and $\Delta C_{GEM}/_{\Delta z}$ is the concentration gradient of the trace gas (for GEM in units of $nanogram \cdot meter^{-4}$). Determination of K is performed by the aerodynamic method, whereby K parameterization involves Monin–Obukhov similarity theory and is calculated directly from sonic anemometer measurements (30) according to the following equation:

**Table 2. Calculation of annual litterfall at Harvard Forest based on a 10-y record of litterfall mass measured at the site and end-of-season Hg analyses of foliar samples of four dominant tree species**

| Species | Annual biomass litterfall ($Mg \cdot ha^{-1}$)* | Litterfall mercury concentration ($\mu g \cdot kg^{-1}$)† | Litterfall mercury deposition ($\mu g \cdot m^{-2}$) |
|---|---|---|---|
| Oak | 234 | 16.9 | 3.9 |
| Maple | 112 | 23.3 | 2.6 |
| Beech | 32 | 34.1 | 1.1 |
| Hemlock | 20 | 22.2 | 0.4 |
| Total | 398 | 20.4‡ | 8.1 |

*Based on measured annual litterfall from 2000 to 2007, averaging 1.99 $Mg \cdot C \cdot ha^{-1}$ (3.98 $Mg \cdot biomass \cdot ha^{-1}$). Annual litterfall was separated into four dominant species based on observed litterfall contributions and scaled up to 100% (Oak: 59%, Maple: 28%, Beech: 8%, and Hemlock: 5%).
†Foliage concentrations at the end of the growing season (September 2018).
‡Weighted average mean concentration.

$$K = \frac{u^* k(z-d)}{\phi_m},$$

where k is the Karman constant (0.4), u* is the friction velocity, z and d are measurement height above ground and zero-plane displacement height, respectively, and $\phi_m$ is the diabatic influence function for momentum. Trace gas flux footprints that contribute to the formation of the concentration profile at a sensor location are dependent on atmospheric stability and generally originate within 500 m distance to the measurement tower. Flux-gradient methods assume that no sources or sinks of the trace gas of interest exist between the two gradient inlets. For GEM, we consider this a valid assumption given that GEM has an atmospheric residence time of several months (47) and is highly stable within the short time of turbulent exchange within canopies (minutes to hours). It is unlikely that concentrations of GOM impact gradients given that concentrations are 300 times lower than GEM (*SI Appendix*, Fig. S6) and show low breakthrough with the inlet configuration used (48).

An EC system measured fluxes of $CO_2$, $H_2O$, momentum, and sensible and latent heat at 29 m with a closed-path infrared gas analyzer (IRGA; Model 6261, LI-COR, Lincoln, Nebraska) sampling air to measure $CO_2$ and $H_2O$ at 4 Hz frequency. The IRGA was calibrated three times daily by standard addition of $CO_2$. Vertical and horizontal wind speed and air temperature were measured at 29 m using a three-axis orthogonal array sonic anemometer (Applied Technologies Inc., Longmont, Colorado) reporting at 8 Hz. An additional sonic anemometer (Model 81000, R. M. Young Company, Traverse City, Michigan) was deployed for measurement of forest floor GEM fluxes at a height of 1.9 m.

Above-forest GEM gradients were measured at heights of 24.1 m and 30.8 m (and 29 m before May 15, 2019). Forest-floor GEM gradients were measured at 0.4 m and 1.2 m above the ground. Two pairs of air inlets each (total of four inlet lines) were used to draw air to instruments inside the field laboratory through 1/4" perfluoroalkoxy (PFA) tubes and 47-mm PFA inlet filter holders and 0.2-μm PFA inlet filters. Inlet filters were changed every one to three months and lines were wrapped for light protection to avoid photochemical reactions. Two valve control systems with three-way solenoid valves with Teflon-wetted flow paths (NResearch, West Caldwell, NJ) were used to switch between the two gradient inlets every 10 min and allowing a concentration measurement with each of the two sampling traps of the analyzers (traps A and B) at each inlet height, therefore avoiding trap biases. Lines not being sampled were flushed by a pump to avoid stagnant air in lines. Two ambient air mercury analyzers (Model 2537B and 2537X, Tekran Inc., Toronto, Canada) were used for gradient measurements, one for above-canopy (whole-ecosystem) fluxes and one for forest-floor GEM fluxes. We used internal calibration systems to perform autocalibrations every 49 h. Internal calibrations were verified prior to and after field deployments with an independent calibration source (Model 2500, Tekran Inc.). In order to prevent systematic errors in GEM gradients due to null gradients, the sampling lines and inlets were tested for contamination during regular field visits (every 2 to 4 wk) by routing mercury-free air to the sample inlets. In addition, the entire sampling trains were rotated between the two inlet heights on average every 40 d to test for null gradients.

For data quality procedures of ecosystem GEM fluxes, we performed an outlier removal of the raw dataset containing 18,501 30-min GEM concentration differences and subsequently calculated 11,314 30-min GEM flux data points when micrometeorological variables were available and conditions valid to apply the flux-gradient method (not considering periods of highly stabile or highly unstable conditions, [i.e., when z/L<-2 or z/L > 1]). A second outlier removal was performed for calculated fluxes, which reduced the flux dataset to 10,319 30-min data points. For calculation of cumulative flux graphs, we interpolated missing values using respective median monthly values for hourly summarized data. To verify the flux gradient approach, we compared $CO_2$ fluxes using the flux-gradient method with fluxes correspondingly measured by EC during summer and fall 2019, and we observed good agreements in magnitudes and directions of $CO_2$ fluxes measured by the two approaches (*SI Appendix*, Fig. S4). Random error analysis of GEM fluxes was performed using a "daily differencing approach," and flux uncertainties were propagated for calculation of cumulative sums using the frequency distribution of random errors (*SI Appendix*, Fig. S5).

**Data Availability.** Raw and processed flux data have been deposited in the Environmental Data Initiative at https://doi.org/10.6073/pasta/0d9d994b069bc1d2a11eb9a7dc783bff (49).

**ACKNOWLEDGMENTS.** We thank John Budney, Mark van Scoy, and Dean Howard for help for set-up and maintenance of the measurement and tower system and support of field measurements. We thank Max Berkelhammer for the loan of instrumentation at Harvard Forest. Funding for this project was provided by US NSF (Division of Atmospheric and Geospace Sciences awards [AGS] #1848212 and #1848618 and Division of Envionmental Biology award [DEB] #2027038). Additionally, the flux tower operations are supported by the US Department of Energy through the Lawrence Berkeley Nationals Laboratory for support of AmeriFlux core sites (DE-AC02-05CH11231) and by the NSF for the Harvard Forest Long-Term Ecological Research (DEB-1832210). This is Lamont Contribution No. 8494.

1. C. T. Driscoll, R. P. Mason, H. M. Chan, D. J. Jacob, N. Pirrone, Mercury as a global pollutant: Sources, pathways, and effects. *Environ. Sci. Technol.* **47**, 4967–4983 (2013).
2. J. D. Demers, J. D. Blum, D. R. Zak, Mercury isotopes in a forested ecosystem: Implications for air-surface exchange dynamics and the global mercury cycle. *Global Biogeochem. Cycles* **27**, 222–238 (2013).
3. M. Jiskra *et al*., Mercury deposition and re-emission pathways in boreal forest soils investigated with Hg isotope signatures. *Environ. Sci. Technol.* **49**, 7188–7196 (2015).
4. D. Obrist *et al*., Tundra uptake of atmospheric elemental mercury drives Arctic mercury pollution. *Nature* **547**, 201–204 (2017).
5. W. Zheng, D. Obrist, D. Weis, B. A. Bergquist, Mercury isotope compositions across North American forests. *Global Biogeochem. Cycles* **30**, 1475–1492 (2016).
6. J. Zhou, D. Obrist, A. Dastoor, M. Jiskra, A. Ryjkov, Mercury uptake by vegetation and impacts on global mercury cycling. *Nat. Rev. Earth and Environ.* **2**, 1–16 (2021) in press.
7. D. Obrist *et al*., A review of global environmental mercury processes in response to human and natural perturbations: Changes of emissions, climate, and land use. *Ambio* **47**, 116–140 (2018).
8. X. Wang, Z. Bao, C.-J. Lin, W. Yuan, X. Feng, Assessment of global mercury deposition through litterfall. *Environ. Sci. Technol.* **50**, 8548–8557 (2016).
9. J. Munthe, H. Hultberg, A. Iverfeldt, Mechanisms of deposition of methylmercury and mercury to coniferous forests. *Water Air Soil Pollut.* **80**, 363–371 (1995).
10. Y. Agnan, T. Le Dantec, C. W. Moore, G. C. Edwards, D. Obrist, New constraints on terrestrial surface atmosphere fluxes of gaseous elemental mercury using a global database. *Environ. Sci. Technol.* **50**, 507–524 (2016).
11. J. Bieser *et al*., Multi-model study of mercury dispersion in the atmosphere: Vertical and interhemispheric distribution of mercury species. *Atmos. Chem. Phys.* **17**, 6925–6955 (2017).
12. J. O. Bash, D. R. Miller, Growing season total gaseous mercury (TGM) flux measurements over an *Acer rubrum* L. stand. *Atmos. Environ.* **43**, 5953–5961 (2009).
13. S. Lindberg, P. Hanson, T. Meyers, K. Kim, Air/surface exchange of mercury vapor over forests—The need for a reassessment of continental biogenic emissions. *Atmos. Environ.* **32**, 895–908 (1998).
14. Q. Yu *et al*., Gaseous elemental mercury (GEM) fluxes over canopy of two typical subtropical forests in south China. *Atmos. Chem. Phys.* **18**, 495–509 (2018).
15. L. P. Wright, L. Zhang, F. J. Marsik, Overview of mercury dry deposition, litterfall, and throughfall studies. *Atmos. Chem. Phys.* **16**, 13399–13416 (2016).
16. A. Finzi *et al*., Carbon budget of the Harvard Forest Long-Term Ecological Research site: Pattern, process, and response to global change. *Ecol. Monogr.* **90**, 1–37 (2020).
17. G. C. Edwards *et al*., Development and evaluation of a sampling system to determine gaseous mercury fluxes using an aerodynamic micrometeorological gradient method. *J. Geophys. Res. Atmos.* **110**, 1–11 (2005).
18. B. E. Law *et al*., Environmental controls over carbon dioxide and water vapor exchange of terrestrial vegetation. *Agric. For. Meteorol.* **113**, 97–120 (2002).
19. A. G. Millhollen, M. S. Gustin, D. Obrist, Foliar mercury accumulation and exchange for three tree species. *Environ. Sci. Technol.* **40**, 6001–6006 (2006).
20. J. A. Graydon, V. L. St Louis, S. E. Lindberg, H. Hintelmann, D. P. Krabbenhoft, Investigation of mercury exchange between forest canopy vegetation and the atmosphere using a new dynamic chamber. *Environ. Sci. Technol.* **40**, 4680–4688 (2006).
21. M. Jiskra *et al*., A vegetation control on seasonal variations in global atmospheric mercury concentrations. *Nat. Geosci.* **11**, 244–250 (2018).
22. D. Obrist, Atmospheric mercury pollution due to losses of terrestrial carbon pools? *Biogeochemistry* **85**, 119–123 (2007).
23. V. L. St Louis *et al*., Atmospheric concentrations and wet/dry loadings of mercury at the remote experimental lakes area, Northwestern Ontario, Canada. *Environ. Sci. Technol.* **53**, 8017–8026 (2019).
24. W. Yuan *et al*., Stable isotope evidence shows re-emission of elemental mercury vapor occurring after reductive loss from foliage. *Environ. Sci. Technol.* **53**, 651–660 (2019).
25. W. Zhu *et al*., Global observations and modeling of atmosphere-surface exchange of elemental mercury: A critical review. *Atmos. Chem. Phys.* **16**, 4451–4480 (2016).
26. D. Obrist, A. K. Pokharel, C. Moore, Vertical profile measurements of soil air suggest immobilization of gaseous elemental mercury in mineral soil. *Environ. Sci. Technol.* **48**, 2242–2252 (2014).
27. A. K. Pokharel, D. Obrist, Fate of mercury in tree litter during decomposition. *Biogeosciences* **8**, 2507–2521 (2011).
28. J. D. Demers, C. T. Driscoll, T. J. Fahey, J. B. Yavitti, Mercury cycling in litter and soil in different forest types in the Adirondack region, New York, USA. *Ecol. Appl.* **17**, 1341–1351 (2007).
29. B. D. Hall, V. L. St Louis, Methylmercury and total mercury in plant litter decomposing in upland forests and flooded landscapes. *Environ. Sci. Technol.* **38**, 5010–5021 (2004).
30. L. K. Meredith *et al*., Ecosystem fluxes of hydrogen: A comparison of flux-gradient methods. *Atmos. Meas. Tech.* **7**, 2787–2805 (2014).

31. J. Fritsche *et al*., Elemental mercury fluxes over a sub-alpine grassland determined with two micrometeorological methods. *Atmos. Environ.* **42**, 2922–2933 (2008).
32. M. S. Castro, C. W. Moore, Importance of gaseous elemental mercury fluxes in Western Maryland. *Atmosphere (Basel)* **7**, 1–13 (2016).
33. S. Osterwalder *et al*., Mercury evasion from a boreal peatland shortens the timeline for recovery from legacy pollution. *Sci. Rep.* **7**, 16022 (2017).
34. NADP, National Atmospheric Deposition Program (NADP): About the NADP Concentration and Deposition Maps (2020). http://nadp.slh.wisc.edu/newissues/litterfall/. Accessed 16 November 2020.
35. L. Zhang, P. Zhou, S. Cao, Y. Zhao, Atmospheric mercury deposition over the land surfaces and the associated uncertainties in observations and simulations: A critical review. *Atmos. Chem. Phys.* **19**, 15587–15608 (2019).
36. NADP, National Atmospheric Deposition Program (NADP): Litterfall Mercury Monitoring Initiative (2020). http://nadp.slh.wisc.edu/mdn/. Accessed 16 November 2020.
37. M. R. Risch *et al*., Spatial patterns and temporal trends in mercury concentrations, precipitation depths, and mercury wet deposition in the North American Great Lakes region, 2002-2008. *Environ. Pollut.* **161**, 261–271 (2012).
38. X. Wang *et al*., Underestimated Sink of Atmospheric Mercury in a Deglaciated Forest Chronosequence. *Environ. Sci. Technol.* **54**, 8083–8093 (2020).
39. L. P. Wright, L. Zhang, F. J. Marsik, Overview of mercury dry deposition, litterfall, and throughfall studies. *Atmos. Chem. Phys.* **16**, 13399–13416 (2016).
40. D. Obrist *et al*., A synthesis of terrestrial mercury in the western United States: Spatial distribution defined by land cover and plant productivity. *Sci. Total Environ.* **568**, 522–535 (2016).
41. D. Smith, W. Cannon, L. G. Woodruff, F. Solano, K. J. Ellefsen, "*Geochemical and mineralogical maps for soils of the conterminous United States*" (U.S. Department of the Interior, U.S. Geological Survey Open-File Rep. 2014–1082, 2014), https://doi.org/10.3133/ofr20141082, p. 386.
42. M. Jiskra, J. G. Wiederhold, U. Skyllberg, R. M. Kronberg, R. Kretzschmar, Source tracing of natural organic matter bound mercury in boreal forest runoff with mercury stable isotopes. *Environ. Sci. Process. Impacts* **19**, 1235–1248 (2017).
43. M. R. Turetsky *et al*., Wildfires threaten mercury stocks in northern soils. *Geophys. Res. Lett.* **33**, 6 (2006).
44. K.E. Moore *et al*., Seasonal variation in radiative and turbulent exchange at a deciduous forest in Central Massachusetts. *J. Appl. Meteorol.* **35**, 122–134 (1996).
45. M. L. Goulden, J. W. Munger, S. M. Fan, B. C. Daube, S. C. Wofsy, Measurements of carbon sequestration by long-term eddy covariance: Methods and a critical evaluation of accuracy. *Glob. Change Biol.* **2**, 169–182 (1996).
46. T. Meyers, M. Hall, S. Lindberg, K. Kim, Use of the modified Bowen-ratio technique to measure fluxes of trace gases. *Atmos. Environ.* **30**, 3321–3329 (1996).
47. W. H. Schroeder, J. Munthe, Atmospheric mercury—An overview. *Atmos. Environ.* **32**, 809–822 (1998).
48. C. W. Moore, D. Obrist, M. Luria, Atmospheric mercury depletion events at the Dead Sea: Spatial and temporal aspects. *Atmos. Environ.* **69**, 231–239 (2013).
49. D. Obrist, W. Munger, R. Commane, Atmospheric Gaseous Elemental Mercury Fluxes at Harvard Forest EMS Tower 2019-2020. *Environmental Data Initiative*. https://doi.org/10.6073/pasta/0d9d994b069bc1d2a11eb9a7dc783bff. Deposited 29 June 2021.